Journal of Power Sources 436 (2019) 226835

Contents lists available at ScienceDirect

Journal of Power Sources

journal homepage: www.elsevier.com/locate/jpowsour

Fast and safe charging method suppressing side reaction and lithium deposition reaction in lithium ion battery

Minseok Song, Song-Yul Choe *

Mechanical Engineering, 1418 Wiggins Hall, Auburn University, AL, 36849, USA

HIGHLIGHTS

- Propose a safe and fast charging method based on a reduced electrochemical model.
- Analysis of battery degradation from side reaction, lithium plating and stripping.
- Design charging profile considering different limitations with negative pulse.
- Verify the charging method in real time using the Battery-In-The-Loop system.
- Reduce the charging time while maintaining the degradation speed.

GRAPHICAL ABSTRACT

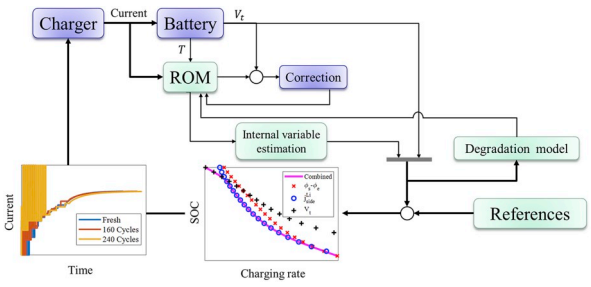

ARTICLE INFO

Keywords:
Lithium ion battery
Fast charging method
Reduced order electrochemical model
Side reaction
Lithium plating
Lithium stripping
Charging time
Pulse charging
Degradation speed

ABSTRACT

Previously published work on fast charging method has demonstrated that the side reaction can be minimized by a properly designed charging protocol, but does not consider effect of lithium plating and stripping. Therefore, a model for side reaction, lithium plating, and stripping is developed and incorporated into a reduced order electrochemical model (ROM) with extended Kalman filter. In addition, effects of negative pulse charging are analyzed and show that negative pulse charging can recover ions from metallic lithium, so the capacity loss is minimized compared with CC charging with the same charging speed. Finally, a new fast charging method is designed by combining negative pulse and different limitations that include anode potential, side reaction rate and cutoff voltage that are estimated from ROM, which is called a fast charging method with negative pulse (FCNP). The proposed method, 2C and 3C CC/CV charging methods are tested in Battery-In-The-Loop using a large format pouch type lithium ion battery. The charging time by FCNP up to 80% SOC is comparable to that by 3C CC/CV at the beginning of life and faster after the middle of life. At the same time, the capacity loss by FCNP is comparable to that by 2C CC/CV.

1. Introduction

Lithium ion battery is one of the most preferred energy storage devices because of its high energy and power density [1]. However, since the driving range of EVs is still relatively short, more batteries are installed to extend the range, which results in long charging time. The charging time can be reduced simply by increased C rates that adversely accelerate degradation, which presents one of the major barriers to overcome for rapid commercialization of EVs. In our previous work, a new fast charging method is proposed that significantly reduce the charging time while degradation is comparable to that by a normal 1C CC/CV charging, by generating a charging protocol considering allowable maximal ion concentration and side reaction rates, and terminal

* Corresponding author.
E-mail addresses: mms0086@auburn.edu (M. Song), choeson@auburn.edu (S.-Y. Choe).

https://doi.org/10.1016/j.jpowsour.2019.226835
Received 14 March 2019; Received in revised form 27 June 2019; Accepted 30 June 2019
Available online 10 July 2019

Nomenclatures

A	sandwich area of the cell (cm^2)
a_α	anodic intercalation factor
a_c	cathodic intercalation factor
$a_{s,side}$	specific surface area of side reaction at electrode (cm^{-1})
$a_{s,Li}$	specific surface area of lithium deposition reaction at electrode (cm^{-1})
BIL	Battery-In-the-Loop
c	ion concentration (mol L^{-1})
CC	Constant Current
CP	Constant Power
CV	Constant Voltage
ch	Charge
D_s	diffusion coefficient in electrode ($cm^2\ s^{-1}$)
D_e	diffusion coefficient in electrolyte ($cm^2\ s^{-1}$)
dis	Discharge
DL	Deposit Layer
EC	Ethylene Carbonate
EIS	Electrochemical Impedance Spectroscopy
EKF	Extended Kalman Filter
F	Faraday constant (96,487 C mol^{-1})
FC	Fast Charging
FCNP	Fast Charging with Negative Pulse
FOM	Full Order Model
I	current of the cell (A)
i_0	exchange current density (A cm^{-2})
j	reaction rate (A cm^{-3})
L	thickness of micro cell (cm)
l	coordinate along the thickness of micro cell
n_{side}	number of ions involved in the side reaction
OCV	Open Circuit Voltage (V)
PC	Pulse Charging
Q	capacity of the cell (A h)
q_{loss}	amount of ion loss caused by degradation (A h)
R	resistance ($\Omega\ cm^2$) or universal gas constant (8.3143 J $mol^{-1}\ K^{-1}$)
R_s	radius of spherical electrode particle (cm)
RMS	Root Mean Square
ROM	Reduced Order Model
r	coordinate along the radius of electrode particle (cm)
SOC	State Of Charge
SEI	Solid Electrolyte Interphase
SEI,sec	Secondary SEI layer
T	cell temperature (K)
t	time (s)
U_{eq}	equilibrium potential (V)
V_t	terminal voltage of cell (V)
x	stoichiometric number of the anode
y	stoichiometric number of the cathode

Greek symbols

α	transfer coefficient of reaction
δ	thickness (mm)
ε	volume fraction of a porous medium or strain
ϕ	electric potential (V)
η	reaction overpotential of electrode (V)
κ	ionic conductivity (S cm^{-1})
λ	ratio of plated lithium and generation of secondary SEI layer
σ	conductivity (S cm^{-1})
τ	total time (s)

Subscripts and Superscripts

a	Anodic
aged	aged cell
ave	average value
c	Cathodic
e	electrolyte phase
eff	Effective
eq	Equilibrium
fresh	fresh cell
loss	caused by loss of lithium ion
Li	lithium ion
LiP	lithium plating
LiS	lithium stripping
max	Maximum
s	solid phase
side	side reaction
surf	electrode particle surface
–	negative electrode (anode)
+	positive electrode (cathode)

cutoff voltage [29]. However, the charging method does not consider any conditions that suppress formation of lithium plating and promote lithium stripping.

In this paper, we propose a fast and safe charging protocol that limits side reaction and lithium plating by side reaction rate, anode potential, and terminal cutoff voltage. The immeasurable internal variables from the terminal of a cell are estimated in real time using a validated electrochemical model. In addition, negative pulse currents are applied to recover lithium ions out of metallic lithium, particularly at low SOC range.

1.1. Review of current charging protocols

There are many suggestions on how to design charging methods that reduce charging time and at the same time degradation. A study conducted by U.S. Army research laboratory showed the fact that charging protocols (constant current (CC) charging, constant power (CP) charging, and multistage constant current (MCC) charging) for lithium ion battery have a significant impact on their cycle life [2]. One of the most commonly used charging protocols is the constant current and constant voltage (CC/CV) charging because of its simple and easy implementation to chargers. During the constant current charging, a cell is charged with a preset current amplitude until the terminal voltage reaches a cutoff voltage set. Once the voltage reaches the cutoff voltage, the applied voltage is kept as constant and then the charging current decreases as the SOC increases. The charging time cannot be significantly reduced by increased constant current because the cutoff voltage is reached earlier and correspondingly an extra time is required during the following CV charging. Other options are constant power and constant voltage charging (CP/CV) or multistage constant current and constant voltage charging (MCC/CV), where the amplitude of the charging current and its duration is hard to determine. A new design of protocols is approached using electric equivalent circuit models or neural network models constructed using experimental data [3] in conjunction with extended Kalman filter [4]. However, empirical models do not provide internal physical variables. Therefore, the variables are extracted from a reduced order electrochemical model (ROM). According to the previous studies on fast charging methods [28,29], there are several limitations for charging current rates at a given SOC that include side reaction rate, terminal cutoff voltage, and lithium ion surface concentration. In addition, resting pulses are added to decrease the surface concentration of lithium ions. However, these methods do

not consider the degradation caused by lithium plating that is the most dominant cause at high current charging. Further studies have been focused on understanding of the effects of charging currents on lithium deposition reaction so that a charging protocol can be designed that suppresses the lithium plating.

1.2. Review of aging mechanisms

Aging phenomena of lithium ion battery are very complex, affected by an electrochemical reaction, heat generated and mechanical stress. The most dominant causes are by electrochemical reactions that include side reaction and lithium deposition reaction. In this study, two reactions are considered as the side reactions as follows [5];

$$2Li^{+}+2e^{-}+EC\rightarrow CH2 == CH2+Li_2CO_3\downarrow \quad (1)$$

$$2Li^{+}+2e^{-}+2EC\rightarrow CH2 == CH2+(CH_2OCO_2Li)_2\downarrow \quad (2)$$

Main products are Li_2CO_3 and $(CH_2OCO_2Li)_2$ that form the compounds of a thin passive layer on anode particle surface that is called Solid Electrolyte Interphase (SEI). An initial SEI is artificially created to protect the electrode from further reaction with the electrolyte because of its permeability to lithium ion but impermeability to electrons [6]. However, as cycled, side reaction takes place continuously and produces the SEI layer that covers pores of the electrode [7,8]. As a result, electrode porosity gets decreased [9] and internal impedance gets increased. Consequently, power gets faded. The lithium ions consumed by the side reaction and trapped in isolated particles due to being completely covered by SEI layers leads to capacity fade.

Lithium deposition reaction that is also called lithium plating forms a metallic solid lithium from the lithium ions and electrons, which can be expressed as follows;

$$Li^{+}+e\rightarrow Li(s) \quad (3)$$

The lithium plating consumes lithium ions, while the metallic plate covers the surface of particles on anode electrode and reduces an active area. In addition, some plated lithium metal reacts with the electrolyte and becomes insoluble products such as Li_2CO_3 and $(CH_2OCO_2Li)_2$, which is called secondary SEI [12,13]. The products can block the pores, reduce ionic kinetics [14] and active anode material [15], which also leads to power and capacity fade. Due to both reactions, the thickness of SEI grows, a conductivity of electrolytes decreases and a layer is formed by a new SEI and the secondary SEI at an interface between anode and separator that is called a deposit layer. All of the depositions are summarized with two impedances, SEI, and deposit layer. The decrease of the active area and the increases of the two resistances are the main causes of degradation. On the other hand, there is a reverse reaction of lithium deposition reaction, which is lithium dissolution reaction also called lithium stripping. A certain amount of the plated lithium can be dissolved during discharge and this reaction promotes recovering ions that are lost during lithium plating [23]. For modeling of side reaction and lithium plating effects, the following assumptions have been made;

- Degradation takes place only on the anode electrode and depositions on the anode particles are a mixture of primary and secondary SEI layer, and plated lithium,
- Products of the primary and secondary SEI layer is composed of Li_2CO_3 and $(CH_2OCO_2Li)_2$,
- Decrease of active area and porosity is calculated from the average thickness of the deposits, and
- Mechanical failure, gas generation, and effect of dendrite are not considered.

Schematic diagram of a graphite particle on the anode electrode is depicted in Fig. 1, where arrows indicate the path of participating charges that includes lithium ion, EC, and electron and the location where reactions take place. Since the SEI layer is ionic conductive but isolative to electrons [6], all reactions that include the main reaction, side reaction, and lithium deposition reaction take place at the interface between the SEI layer and the particle. On the other hand, once lithium metal is deposited on the particle surface, no ion can be transported through plated lithium because of its permeability to ions but impermeability to ions. As a result, no further main reaction is possible. However, electrons in the particles can flow through plated lithium and participate in side reaction or lithium plating on the surface of the plated lithium. Even if the SEI layer or secondary SEI layer on the plated lithium already exist, it is still possible for additional SEI layer or secondary SEI layer to build at the interface of the plated lithium and SEI layer.

2. Degradation mechanism

2.1. Main reaction

Reaction rate produced by a main chemical reaction taking place at the interface between electrode and electrolyte is governed by the Butler-Volmer equation [16].

$$j_{int}^{Li}=a_{s,int}i_{0,int}\left[\exp\left(\frac{\alpha_a F}{RT}\eta_{int}\right)-\exp\left(-\frac{\alpha_c F}{RT}\eta_{int}\right)\right] \quad (4)$$

, where $a_{s,int}$ is the specific reaction area of intercalation, η_{int} is the surface overpotential, and $i_{0,int}$ is the exchange current density of the intercalation that can be expressed as follows;

$$i_{0,int}=k_{i0}(c_e)^{\alpha_a}\left(c_{s,\max}-c_{s,surf}\right)^{\alpha_a}\left(c_{s,surf}\right)^{\alpha_c} \quad (5)$$

, where k_{i0} is the kinetic rate constant, $c_{s,\max}$ and $c_{s,surf}$ are the maximum lithium ion concentration and surface ion concentration of the particles, respectively. α_a and α_c are constants that represent anodic and cathodic intercalation, which are symmetric in the main reaction and set as 0.5 for each value. The overpotential for the main intercalation is given as follows;

$$\eta_{int}=\phi_s-\phi_e-U_{eq,int}-V_{SEI,int} \quad (6)$$

$$V_{SEI,int}=\frac{R_{SEI,total}}{a_{s,int}}j_{total}^{Li} \quad (7)$$

where ϕ_s and ϕ_e are electric potential of the surface of the anode electrode particle and the electrolyte, respectively. $U_{eq,int}$ is the equilibrium potential for the intercalation. j_{total}^{Li} is the total reaction rate that includes the main reaction, the side reaction, and the lithium deposition reaction or the lithium dissolution reaction;

$$j_{total}^{Li}=j_{int}^{Li}+j_{side}^{Li}+j_{Li}^{Li} \quad (8)$$

$R_{SEI,total}$ is the sum of the SEI and the secondary SEI resistance. $R_{SEI,0}$ is the SEI resistance formed at initial cycle, which is measured by electrochemical impedance spectroscopy (EIS) equipment.

$$R_{SEI,total}(\tau)=R_{SEI,0}+R_{SEI}(\tau)+R_{SEI,sec}(\tau) \quad (9)$$

2.2. Side reaction

The rate of side reaction can be also expressed using the BV equation.

$$j_{side}^{Li}=a_s i_{0,side}\left[\exp\left(\frac{\alpha_{a,side}n_{side}F}{RT}\eta_{side}\right)-\exp\left(-\frac{\alpha_{c,side}n_{side}F}{RT}\eta_{side}\right)\right] \quad (10)$$

, where $i_{0,side}$ is the exchange current density of the side reaction that is a function of reactants of the side reaction, lithium ions, and ethylene carbonate (EC) molecules.

$$i_{0,side}=k_{side}\sqrt{c_{s,surf}c_{EC,R_s}} \quad (11)$$

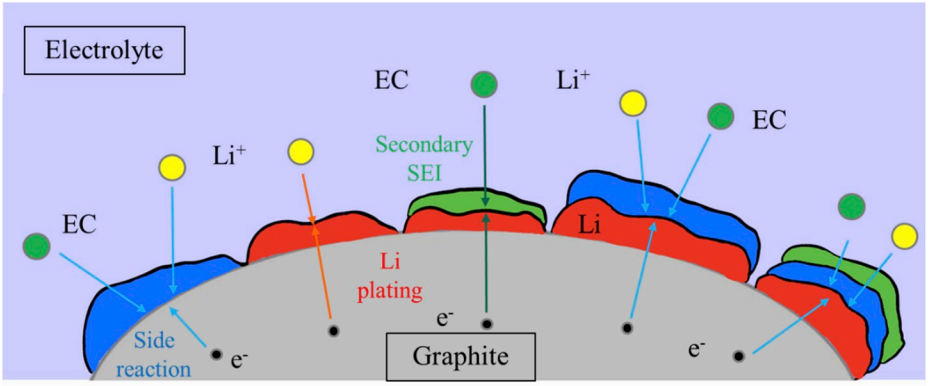

Fig. 1. Schematic diagram of different types of depositions on a graphite particle.

, where k_{side} is the kinetic rate constant for the side reaction. c_{EC,R_s} is the concentration of EC molecules at the surface of anode particles.

n_{side} is the number of ions involved in the side reaction that is equal to 2. η_{side} is the surface overpotential of the side reaction defined as follows [17];

$$\eta_{side} = \phi_s - \phi_e - U_{eq,side} - \frac{R_{SEI,total} j^{Li}_{total}}{a_{s,side}} \tag{12}$$

, where $a_{s,side}$ is the specific reaction area of side reaction and $U_{eq,side}$ is the equilibrium potential for the side reaction.

Since the side reaction is irreversible and dominated by the reduction process rather than the oxidation process, the equation (10) can be simplified as follows;

$$j^{Li}_{side} = -a_{s,side} i_{0,side} \exp\left(-\frac{\alpha_{c,side} n_{side} F}{RT} \eta_{side}\right) \tag{13}$$

The total number of the consumed lithium ions is obtained by integration of the side reaction rate over the composite anode and cycling time.

$$q^{SR}_{loss}(\tau) = \int_{x=0}^{\delta_-} \left\{ \int_{t=0}^{\tau} j^{Li}_{side}(x,t) dt \right\} A dx \tag{14}$$

, where q^{SR}_{loss} is the consumed lithium ions, δ_- is the thickness of the composite anode and A is the cross section area of the cell.

On the other hand, the amount of consumed solvents of the electrolyte is reflected with the volume fraction rate of electrolyte as follows;

$$\Delta\varepsilon_{e,side}(\tau) = -\frac{\alpha \tilde{V}_e q^{SR}_{loss}(\tau)}{A\delta_- F} \tag{15}$$

, where $\tilde{V}_e$ is the molar volume of the electrolyte and α is the reaction coefficient of the EC. Under the assumption that the products from side reaction have the same reaction rate, the average value of the consumed solvents of the electrolyte that are 0.5 for Li_2CO_3 and 1 for $(CH_2OCO_2Li)_2$ when one mole of lithium ion is consumed is used for the reaction coefficient of the EC.

Subsequently, the effective diffusivity of the lithium ion in the electrolyte is affected by the change of the electrolyte volume fraction affects as follows;

$$D^{eff}_e = D_e \cdot \varepsilon_e \tag{16}$$

, where ε_e is the porosity that indicates a volume fraction of electrolyte that decreases as degraded.

Similarly, the change of the volume fraction of the active material caused by the deposition of the SEI layer can be described as follows;

$$\Delta\varepsilon_{s,side}(x,\tau) = -\frac{\tilde{V}_{SEI}}{n_{side} F} \int_{t=0}^{\tau} j^{Li}_{side}(x,t) dt \tag{17}$$

The change of the average thickness of the SEI layer at different locations and deposit layer can be expressed as;

$$\Delta\delta_{SEI}(x,\tau) = \frac{\tilde{V}_{SEI}}{a_s n_{side} F} \int_{t=0}^{\tau} j^{Li}_{side}(x,t) dt \tag{18}$$

$$\Delta\delta_{DL,side}(\tau) = \frac{\tilde{V}_{SEI} R_s}{n_{side} F} \int_{t=0}^{\tau} j^{Li}_{side}(\delta_-,t) dt \tag{19}$$

, where $\tilde{V}_{SEI}$ is the molar volume of the SEI layer and R_s is the radius of the anode particle.

The corresponding increase of the resistances for the SEI and deposit layer can be obtained using the ionic conductivity of the SEI and the deposit layer as follows;

$$\Delta R_{SEI}(x,\tau) = \Delta\delta_{SEI}(x,\tau)/\kappa_{SEI} \tag{20}$$

$$\Delta R_{DL}(\tau) = \Delta\delta_{DL,side}(\tau)/\kappa_{DL} \tag{21}$$

2.3. Lithium plating and lithium stripping

2.3.1. Introduction

Lithium plating and stripping are reduction and oxidation reaction process. The rate of lithium plating or stripping can be also expressed using BV equation

$$j^{Li}_{LiP/S} = a_{s,Li} i_{0,Li} \left[\exp\left(\frac{\alpha_{a,Li} F}{RT} \eta_{LiP/S}\right) - \exp\left(-\frac{\alpha_{c,Li} F}{RT} \eta_{LiP/S}\right)\right] \tag{22}$$

, where $i_{0,Li}$ is the exchange current density of the reaction.

In fact, because the secondary SEI is insoluble, the lithium plating and stripping are semi-reversible. Therefore, $\alpha_{c,Li}$ and $\alpha_{a,Li}$ are set to be 0.3 and 0.7 [12,19].

The lithium plating occurs during charging the local lithium plating overpotential against a reference of Li/Li+ is less than 0V, which makes the kinetics of lithium deposition reaction higher than that of the main reaction [10,11].

Conversely, the lithium stripping takes place during discharging. When the short discharging currents are applied during charging (pulse charging), not only concentration of lithium ions are decreased but also plated lithium metal is dissolved and lithium ions are released [23]. If the plated lithium has already reacted with EC and becomes the secondary SEI, the plated lithium cannot be dissolved. If the plated lithium is completely covered by primary or secondary SEI layer, the lithium is no longer dissolved and becomes a dead lithium.

A model for the lithium stripping is developed under the following assumptions;

- Lithium stripping takes place only when plated lithium is already generated.
- If the plated lithium is completely dissolved, no more lithium stripping exists.
- Once the plated lithium reacts with EC and generates the secondary SEI, lithium stripping cannot take place.
- The rate of the secondary SEI formation from lithium plating is constant.

2.3.2. Lithium plating

The overpotential of the lithium plating is expressed by Ref. [30].

$$\eta_{Li} = \phi_s - \phi_e - U_{eq,Li} - \frac{R_{SEI,total}}{a_{s,Li}} j^{Li}_{total} \tag{23}$$

$$\eta_{LiP} = \begin{cases} 0 & for\ \eta_{Li} \geq 0 \\ \eta_{Li} & for\ \eta_{Li} < 0 \end{cases} \text{ for lithium plating}$$

, where $a_{s,Li}$ is the specific active area of the lithium plating that is same as $a_{s,side}$. $U_{eq,Li}$ is the equilibrium potential for lithium plating and stripping and is assumed to be zero because the potential is measured with respect to a lithium metal reference [12].

The total number of ion loss consumed by the lithium plating and the secondary SEI is obtained by integration of the reaction rate over the composite anode during a given time.

$$q^{LiP}_{\text{loss}}(\tau) = \int_{x=0}^{\delta_-} \left\{ \int_{t=0}^{\tau} (1-\lambda) j^{Li}_{LiP}(x,t) dt \right\} A dx \tag{24}$$

$$q^{SEI,\text{sec}}_{\text{loss}}(\tau) = \int_{x=0}^{\delta_-} \left\{ \int_{\tau=0}^{t} \lambda j^{Li}_{LiP}(x,\tau) d\tau \right\} A dx \tag{25}$$

, where λ is the ratio for the amount between the plated lithium and the secondary SEI layer formed from the plated lithium.

The consumed electrolyte by the secondary SEI can be expressed as follows;

$$\Delta\varepsilon_{e,SEI,sec}(\tau) = -\frac{\alpha \tilde{V}_e q^{SEI,\text{sec}}_{loss}(\tau)}{A\delta_- F} \tag{26}$$

, where α is assumed to be the same as that of the side reaction. It also changes the effective diffusivity of the lithium ion from the equation (16).

A volume fraction of active material induced by the plated lithium and the secondary SEI layer is expressed as follows;

$$\Delta\varepsilon_{s,LiP}(x,\tau) = -\frac{\tilde{V}_{Li}}{n_{LiP}F} \int_{t=0}^{\tau} (1-\lambda) j^{Li}_{LiP}(x,t) dt \tag{27}$$

$$\Delta\varepsilon_{s,SEI,sec}(x,\tau) = -\frac{\tilde{V}_{SEI}}{n_{side}F} \int_{t=0}^{\tau} \lambda j^{Li}_{LiP}(x,t) dt \tag{28}$$

, where n_{LiP} is the number of ions involved in the lithium plating that is equal to 1 and $\tilde{V}_{Li}$ is the molar volume of the plated lithium.

Increase of thickness of the secondary SEI layer from the plated lithium can be expressed as;

$$\Delta\delta_{SEI,sec}(x,\tau) = \frac{\tilde{V}_{SEI}}{a_s n_{side}F} \int_{t=0}^{\tau} \lambda j^{Li}_{LiP}(x,t) dt \tag{29}$$

The corresponding increase of the SEI resistance including the SEI and the secondary SEI layer can be expressed from the equation (20).

An increase of thickness of the deposit layer from the plated lithium and the secondary SEI layer can be expressed individually as follows;

$$\Delta\delta_{DL,LiP}(\tau) = \frac{\tilde{V}_{LiP} R_s}{F} \int_{t=0}^{\tau} (1-\lambda) j^{Li}_{LiP}(\delta_-, t) dt \tag{30}$$

$$\Delta\delta_{DL,SEI,sec}(\tau) = \frac{\tilde{V}_{SEI} R_s}{n_{side}F} \int_{t=0}^{\tau} \lambda j^{Li}_{LiP}(\delta_-, t) dt \tag{31}$$

The corresponding increase of the deposit layer resistances including the SEI, the secondary SEI layer, and the plated lithium can be expressed from the equation (21).

2.3.3. Lithium stripping

Likewise, the overpotential for the lithium stripping is defined by

$$\eta_{LiS} = \begin{cases} \eta_{Li} & for\ \eta_{Li} \geq 0 \\ 0 & for\ \eta_{Li} < 0 \end{cases} \text{ for lithium stripping}$$

, where η_{Li} is calculated according to the equation (23). Because of the lithium stripping, the total amount of recovered lithium ions can be obtained by integration of reaction rate over the composite anode and time.

$$q^{LiS}_{\text{recovery}}(\tau) = \int_{x=0}^{\delta_-} \left\{ \int_{\tau=0}^{t} j^{Li}_{LiS}(x,\tau) d\tau \right\} A dx \tag{32}$$

Finally, the total ion loss by the lithium plating and stripping is the sum of individual loss and recovery that is given by the equations (24), (25) and (32);

$$q^{Li}_{\text{loss}}(\tau) = q^{LiP}_{\text{loss}}(\tau) + q^{SEI,\text{sec}}_{\text{loss}}(\tau) + q^{LiS}_{\text{recovery}}(\tau) \tag{33}$$

3. Reduced order electrochemical model (ROM) considering degradation

Analysis and design of a charging protocol considering the degradation require information of internal variables in real time such as ion concentrations, side reaction rate and anode potential that cannot be measured from the terminal of a battery cell. These variables can be estimated only using a validated electrochemical model. Charging or discharging of lithium ion battery involves several processes that include ion transport and reactions. They are migration, diffusion, and intercalation or deintercalacation. The processes are governed by nonlinear or partial differential equations (PDE) that describe physical laws, which is used to construct a full order model (FOM). Solving the equations is very computationally expensive. Thus, the FOM is inappropriate for control purposes in real time even high accuracy. A possible approach is to reduce the order of the FOM by converting PDEs into ODEs and linearize the nonlinear equations, which is called a reduced order electrochemical model (ROM). Details of the equations are summarized in Appendix A.

3.1. Model validation

The constructed ROM embedding side reaction and lithium deposition reaction model is validated using a large format of lithium ion pouch cell that has a nominal capacity of 39Ah. The values of the parameters for the ROM is listed in Appendix B.

Firstly, the cell is cycled with 2C CC/CV charging until the terminal voltage reaches the cutoff voltage of 4.2V, where the cutoff current becomes 1/40C, and then discharged with 1C until the terminal voltage reaches 3.0V. The capacity is measured as a function of cycle numbers and the results of capacity and discharge characteristics of terminal voltages from 0 to 320 cycles in every 40 cycles are plotted in Fig. 2. The prediction error of the capacity by the ROM is less than 1% while the voltage is accurately tracked. The capacity drops almost linear until 300 cycles because no lithium plating takes place, which is explored in detail later.

With the degradation model, ion loss is calculated from the side reaction rate. Ion loss from 2C CC/CV charging as a function of cycle number is plotted on the top in Fig. 3. Ion loss increases linearly because

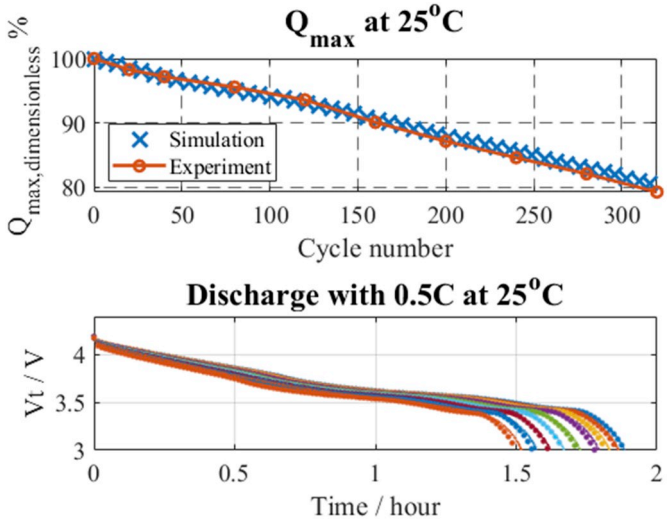

Fig. 2. Experimental and simulated results by 2C CC/CV; capacity fade and terminal voltage when discharged with 0.5C CC.

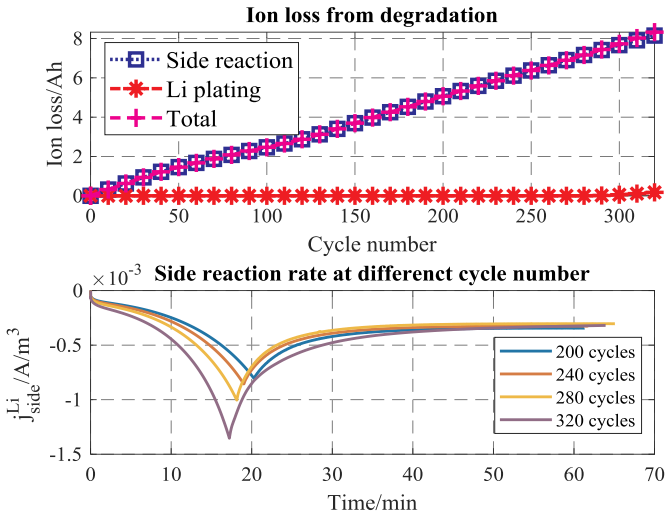

Fig. 3. Ion loss calculated using degradation model and side reaction rate with 2C CC/CV charging.

lithium plating does not occur until 300 cycles and correspondingly, capacity decreases linearly as shown in Fig. 2. Side reaction rates rate at the particle closely located to the separator during one cycling with different cycle number are plotted on the bottom in Fig. 3. Side reaction rate decreases in CV mode as the charging current decreases.

As a matter of fact, high current rates during the charging process is one of the favorable conditions for the formation of lithium plating and thus another cycling test is conducted with 5C CC charging until 40% of SOC for 100 cycles with the same discharge condition. The experimental data of the capacity is compared with that by simulation using the degradation model and ion loss from side reaction and lithium plating are plotted, as shown in Fig. 4, where the model can predict the capacity fade well. In addition, there is a transition from a linear to a nonlinear range caused by the lithium plating [21]. At the beginning of cycling, ion loss is mainly caused by side reaction. After 60 cycles, the lithium plating starts to occur and then increases rapidly, which results in the nonlinear and rapid increase of the capacity loss and a transition from the linear to the nonlinear increase.

This nonlinear transition can be better explained with lithium

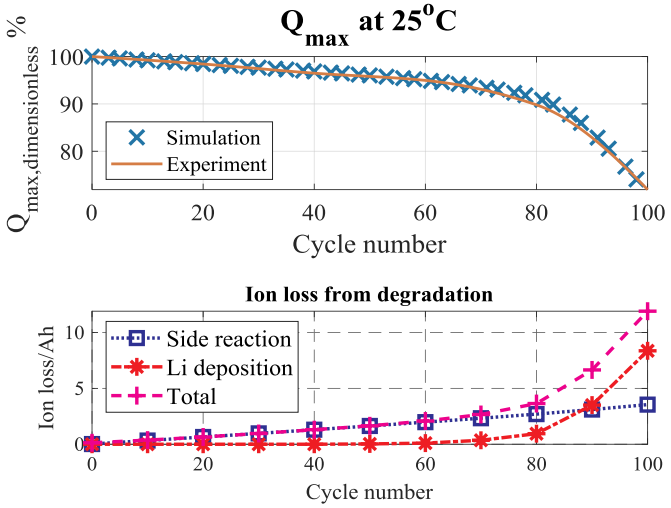

Fig. 4. Capacity fade and ion loss at 5C CC charging by side reaction and lithium plating.

deposition overpotential during charging process that is the primary factor for the formation of the lithium plating according to the BV equation. The lithium deposition overpotential and lithium deposition reaction rate at the particle closely located to the separator as a function of time with different cycle number is plotted in Fig. 5 (a) and (b). When cells are getting aged, the overpotential decreases and becomes negative from 60 cycles, which represents the condition for the formation of lithium plating, consequently lithium deposition reaction rate decreases. As the cycle number increases, more lithium plating takes place, which results in a rapid and nonlinear drop of the capacity. Particularly, the increase of the overpotential and the decrease of the reaction rate at 100 cycles shortly after 250 s is caused by a change of the charging mode from CC to CV because of the degradation and the associated reduced time to reach the cutoff voltage. In addition, because the overpotential is dependent upon the location, the lithium deposition overpotential and the reaction rate at the end of the charging as a function of a location of the particle in the composite anode with different cycle number is plotted in Fig. 5 (c) and (d). The closer the location of particles to the separator is, the lower becomes the overpotential, which causes local lithium deposition reaction. Moreover, when lithium deposition takes place, deposited metallic lithium covers the surface and pores of particles, so volume fraction of the active material decreases, especially severe near the separator. As a result, the closer the location of particles to the separator is, the less is the available active area, which increases the magnitude of the overpotential and accelerates lithium plate like a positive feedback, therefore lithium plating area extends to the opposite direction of the separator.

In short, the design objective of a charging algorithm should be the reduction of the side reaction rate and prevention of lithium deposition reaction, so that few ions can be lost and finally a capacity fade can be minimized. The preventive measure against the lithium deposition reaction results in inhibiting the growth of dendrites, so safer operation can be ensured. Therefore, design objectives have set to develop a charging algorithm that suppresses the side reaction and prevent the lithium plating.

4. Design of a new charging method

4.1. Design of a new fast charging algorithm

The limitations of previously introduced charging method are the side reaction rate and cutoff voltage to minimize the ion loss caused by side reaction [29]. One of the other major causes for degradation is

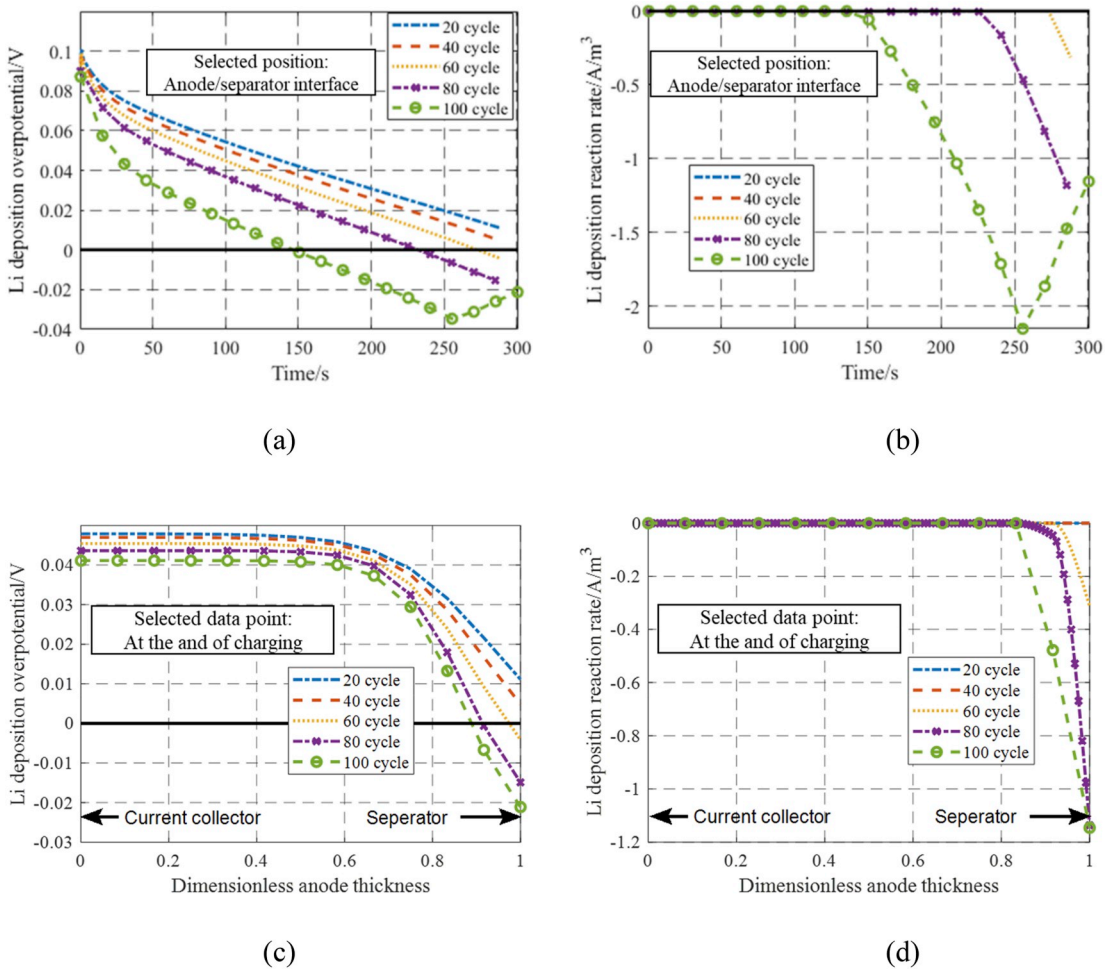

Fig. 5. Lithium deposition overpotential and reaction rate during charging as a function of charging time (a), (b) and location in the anode (c) and (d).

lithium plating that is directly related to negative lithium deposition overpotential, given by equation (23), presents a farvorable condition for the formation of lithium plating, which leads to loss of ions. In this research, anode potential, which is $\phi_s - \phi_e$ used for simplification purpose and actually considering anode potential is more conservative limitation than lithium plating overpotential so that it can reduce degradation comprehensively.

The overall charging process and three limitations for C rates as a function of SOC are calculated using ROM are plotted in Fig. 6 (a), which should minimize the degradation of the cell. The charging starts with the maximum C rate. At an every incremented SOC, the designed algorithm checks if the applying C rates cause any variables to reach the aforementioned three limitations, which is repeated until a required SOC or a certain preset stop condition, such as cutoff current are reached. The cutoff current is set as 1/40C.

When charged from 0% SOC with 8C charging current, the first limitation during the low SOC is the anode potential that should not be lower than the zero voltage and others are the side reaction rate and the terminal cutoff voltage that is 4.2V. Because the high charging current induces extreme heat and hot spots locally that could destroy the thin material in the cell, the maximum charging current is set as 5C. Then at the beginning of life, limitation of anode potential is not considered because limitation of side reaction can always prevent that of anode potential. Based on these constraints, a schematic block diagram of the new fast charging method is depicted in Fig. 6 (b). The ROM continuously compares the simulated voltage with that from measurement to follow the physical internal variables of the battery. Any errors caused by the inaccuracy of the ROM and measurements are further improved by a feedback loop with a correction using Extended Kalman Filter (EKF). The corrected model is used to estimate surface ion concentrations and anode potentials that allow for estimation of SOC, side reaction rate and lithium plating rate, respectively. In addition, a degradation model is incorporated into the ROM and its aging parameters are updated as cycled.

As cycle number increases, the cell gets aged. The aged cell has a decreased volume fraction of electrode and electrolyte that decreases the overpotential that results in enhancing lithium plating and side reaction. Thus, the side reaction rate increases and the anode potential becomes negative, which produces more depositions. Consequently, the Ohmic and SEI resistance increase, which causes a fast increase of the terminal voltage that reaches the cutoff voltage of the cell earlier. Therefore, the charging protocol should be updated as a cell gets aged. Change of allowable C rate at given SOC by cycle number and the updated relationship between SOC and C rate after 160 cycles are plotted in Fig. 6 (c), where the limitation for anode potential changes more than other limitations as aging is progressing. The charging current is primarily limited by the anode potential rather than that of side reaction rate. Therefore, the anode potential is considered at low SOC range. Consequently, the limitation for the charging current is divided into three regions, low SOC range by anode potential, middle range by side reaction rate, and high SOC range by the terminal cutoff voltage.

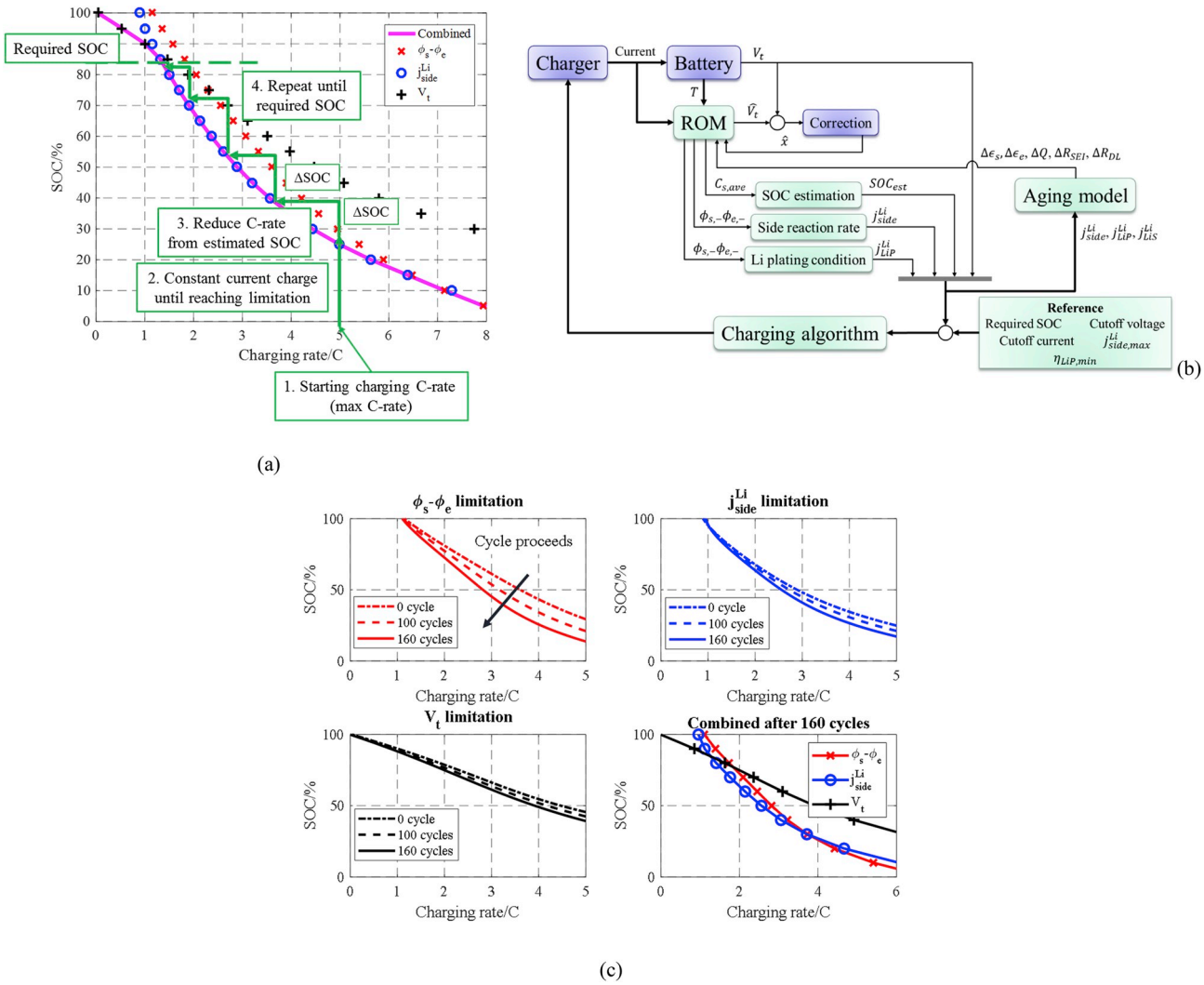

Fig. 6. (a) Different limitations as a function of charging C rates and SOC; (b) Schematic block diagram of proposed fast charging method; (c) Change of SOC vs. C rate as a function of cycles at three different numbers of cycle and updated SOC vs. C rate after 160 cycles.

4.2. Fast charging with negative pulse (FCNP)

Theoretically, no lithium plating should be formed if the anode potential is larger than 0V. In reality, lithium plating could have been formed from the previous cycling or can be formed from any unknown reasons. For such cases, ideally, lithium stripping enables to recover ions out of plated lithium, which can be carried out by discharge pulse currents. In order to study the effects of the discharging current, a cycling tests with 5C CC, 5C CC and 2C negative pulses (NP) with 20 mHz of frequency [26], and 4.3 CC that is the average current of the pulse current are conducted. The profile of the current and voltage during charging is plotted in Fig. 7 (a), where the charging time of 5C CC charging with 2C NP and CC charging with average current are almost identical. The capacity of the three charging methods is measured experimentally and compared with the simulation results from the model, as shown in Fig. 7 (b), where simulation results match experimental results well. Because 5C CC charging can charge the battery faster than the other two methods, degradation speed is the fastest. Up to 60 cycles, the capacity loss is dominantly caused by side reaction and then capacity decreases rapidly because of lithium plating. Comparison between CC charging that has the same average current of the pulse currents and 5C CC with 2C NP has shown that effects of negative pulses are not significant until 100 cycles because lithium plating in the battery charged with average CC charging is not formed yet. When the cycle number is larger than 100 cycles, lithium plating starts to form heavily and then the negative pulse currents take more effective in recovering ions. At the 160 cycles, the charging protocol employing negative pulses has accomplished 14% less capacity fade than that by CC charging.

Since the rate of lithium deposition reaction is a function of the lithium deposition overpotential according to BV equation, the lithium deposition overpotentials from the pulse charging are calculated and plotted over time as a function of cycles in Fig. 7 (c). When negative pulses are applied, the overpotentials tend to follow the pulse form of the current profiles and become positive. At the end of 20 cycles, there is a short period of time where the potential becomes negative, where lithium plating starts to form. As cycle number increases, the formation becomes more frequent, but the positive potentials produced by the negative pulse currents promote lithium stripping. The more lithium plating is formed, the more effective becomes the positive pulse that recovers ions. In addition, the stripping takes more effective at low SOC because the overpotential decreases when SOC becomes high.

Ion loss caused by the side reaction and the lithium plating and ion recovery caused by the lithium stripping are calculated using the validated model and plotted in Fig. 7 (d). Note that the negative value of the ion loss means ions are recovered. Blue line with square symbols indicates ion loss caused by side reaction, red line with star symbols is that

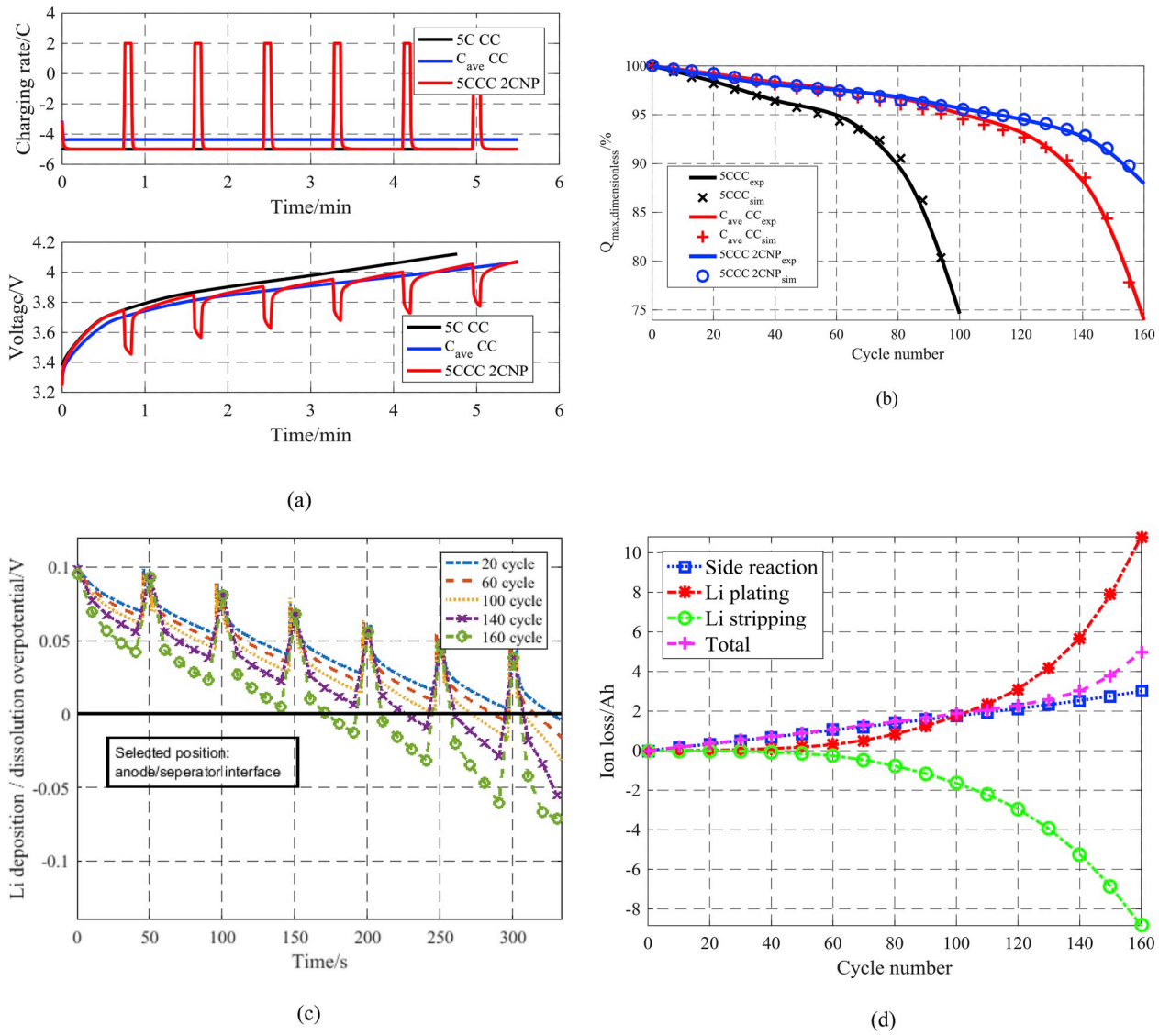

Fig. 7. (a) Comparison of charging current and voltage using 5C CC, average CC and 5C CC with 2C negative pulse charging; (b) Experimental and simulated capacity fade with 5C CC, average CC and 5C CC with 2C negative pulse charging; (c) Lithium deposition and dissolution reaction overpotential during charging 5C CC with 2C negative pulse charging; (d) Ion loss and recovery from side reaction and lithium plating and stripping.

by lithium plating, green line with circle symbols is ion recovery by lithium stripping, and pink line with plus sign symbols is a total sum of ion loss by all reactions. Even though a large number of ions are lost by the lithium plating, negative pulses enable to recover most of them, so the total ion loss using negative pulses is much smaller than that by CC charging with the same average current.

Therefore, adding negative pulses during CC charging allows for minimization of degradation using lithium stripping effects without increasing extra charging time. Afterward, a new charging algorithm combines FC and negative pulse, which is called fast charging with negative pulse (FCNP) is then designed. The FCNP is implemented in BIL and its charging time and capacity fade are compared with those of 2C CC/CV and 3C CC/CV charging.

The three current profiles and their associated SOCs from experiments up to 100% SOC are shown in Fig. 8 (a) and measured and calculated capacity fades are plotted in Fig. 8 (b). In addition, the total amount of energy needed for different charging methods is calculated by integrating the electric power over time, which results in 593.9 kJ for FCNP, 591.4 kJ for 3C CC/CV and 569.0 kJ for 2C CC/CV. In fact, FCNP needs more energy due to negative pulses, which ratio amounts to only 2% of the total energy. Therefore, the energy cost incurring by the negative pulse can be neglected. From the beginning of cycling, the capacity loss by 3C CC/CV charging is always greater than that by FCNP and 2C CC/CV charging and decreases rapidly after 30 cycles, when lithium deposition reaction starts. The proposed FCNP has shown significant improvements. The capacity loss is almost the same as that by 2C CC/CV charging and approximately 23% less than that by 3C CC/CV charging at 60 cycles.

Analysis of the charging time at different SOC intervals summarized in Table 1 has shown that the charging time by FCNP up to 40% SOC becomes 50% less than that by 2C CC/CV and 31% less than that by 3C CC/CV because of the high charging current at low SOC range, as shown in Fig. 8 (a). When charged up to 60% SOC, the charging time by FCNP becomes 43% less than that by 2C CC/CV, and 18% less than that by 3C CC/CV. However, because of low charging current at high SOC range, the charging time after 80% SOC by FCNP takes longer than that by 3C CC/CV.

In fact, the charging time by FCNP up to 100% SOC is longer than 3C CC/CV charging at the beginning of life. However, the 3C CC/CV charging exceeds limitations of charging currents set for lithium plating

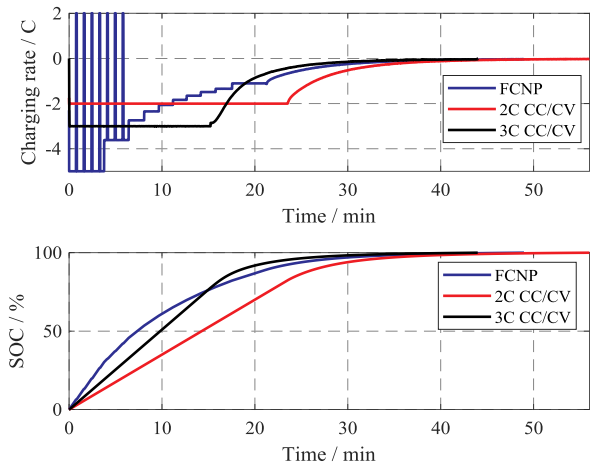

(a)

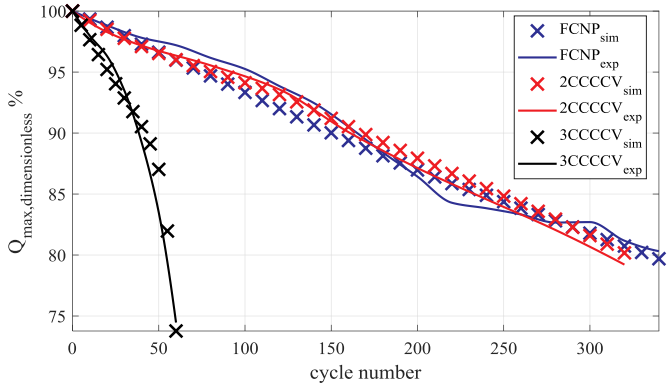

(b)

Fig. 8. (a) Charging response using FCNP, 2C CC/CV, and 3C CC/CV; (b) Capacity loss by FCNP, 2C CC/CV, and 3C CC/CV.

Table 1
Charging time at different SOC intervals using FCNP, 2C CC/CV, and 3C CC/CV.

	40% SOC	60% SOC	80% SOC	100% SOC
FCNP	5.5 min	9.7 min	16.6 min	49.0 min
3C CC/CV	7.9 min	11.8 min	15.7 min	44.0 min
2C CC/CV	11.4 min	17.1 min	22.8 min	56.0 min

Table 2
Charing time up to 100% SOC as a function of cycle number.

	Fresh cell	20 cycles	40 cycles	60 cycles
FCNP	49.0 min	51.1 min	51.1 min	52.0 min
3C CC/CV	44.0 min	47.3 min	53.7 min	55.2 min
2C CC/CV	56.0 min	56.1 min	56.7 min	59.2 min

and side reaction, so degradation is accelerated and the loss of the capacity becomes larger as the cycle number increases. Because the charging time is affected by the aging process. The charging time up to 100% of SOC by three charging methods is measured and compared in Table 2. As expected, the charging time by 3C CC/CV charging is the shortest at BOL, but becomes longer because of fast progress in aging. After 40 cycles, the charging time by FCNP is shorter than two others while capacity fade can be maintained as that by 2C CC/CV charging.

5. Conclusion

A ROM that embeds both side reaction and lithium deposition reaction model is developed and validated against experimental data obtained from a large format pouch type of lithium ion battery. The model is used to analyze the mechanism of the cycle life of the lithium ion battery. In the early stage of cycling, the side reaction is the dominant cause for capacity loss that linearly increases. As the number of cycle increases, lithium deposition reaction takes place, which is the dominant cause for the capacity loss that rapidly increases. Thus, there is a transition of the capacity loss from a linear to a nonlinear range. Reduction of the charging time is simply possible with increased charging currents that accelerate both side reaction and lithium deposition reaction. Therefore, a fast charging protocol is devised to suppress both reactions by limiting side reaction rate and anode potential. Additionally, the effect of discharging pulses on capacity loss is experimentally and numerically analyzed. The added negative pulses on the CC charging protocol promotes lithium stripping, which allows for recovering lithium ions from plated lithium. Consequently, the capacity loss can be decreased and cycle life is extended compared with the classical CC charging protocol that has the same average current as the pulse current. The negative pulse is particularly effective at low SOC range where the amount of ions recovered out of plated lithium is large due to the high lithium stripping overpotential. The proposed fast charging (FCNP) includes negative pulse charging current. Especially, suppression of the lithium plating and removal of plated lithium from lithium stripping through the negative pulses discourages the potential growth of dendrites, which can prevent the internal short and increase the safety of a battery system in operation. The charging time by FCNP is approximately 50% less than 2C CC/CV charging for the interval from 0% to 40% SOC and 43% for the interval 0%–60% SOC, while 31% and 18% less than that 3C CC/CV charging for the interval from 0% to 40% SOC and 60% SOC, respectively. Even though the charging time up to 100% of SOC by FCNP is longer than that by 3C CC/CV charging at BOL, it becomes shorter as degradation is in progress, particularly after 40 cycles. On the other hand, the capacity loss by FCNP is comparable to that by 2C CC/CV charging, which is approximately 23% less than that by 3C CC/CV charging after 60 cycles. Future work includes effects of temperature, particularly at a subzero range where lithium plating severely takes place.

Acknowledgment

This work is funded by Hyundai motor group, Korea. The authors gratefully acknowledge the financial support.

Appendix

Appendix A. Summary of FOM and ROM

Cell dynamics	FOM	ROM
Ion concentration in electrode	$\frac{\partial c_s}{\partial t} = \frac{D_s}{r^2}\frac{\partial}{\partial r}\left(r^2\frac{\partial c_s}{\partial r}\right)$ $\frac{1}{r}\frac{\partial c_s}{\partial r}\Big\|_{r=0} = 0 and D_s\frac{\partial c_s}{\partial r}\Big\|_{r=R_s} = \frac{-j^{Li}}{a_s F}$	$\frac{d}{dt}c_{s,ave} + 3\frac{j^{Li}}{R_s a_s F} = 0$ $\frac{d}{dt}q_{ave} + 30\frac{D_s}{R_s^2}q_{ave} + \frac{45}{2}\frac{j^{Li}}{R_s^2 a_s F} = 0$ $35\frac{D_s}{R_s}(c_{s,surf} - c_{s,ave}) - 8D_s q_{ave} = -\frac{j^{Li}}{a_s F}$
Ion concentration in electrolyte	$\frac{\partial(\varepsilon_e c_e)}{\partial t} = \frac{\partial}{\partial x}\left(D_e^{eff}\frac{\partial}{\partial x}c_e\right) + \frac{1-t_+^0}{F}j^{Li}$ $\frac{\partial c_e}{\partial x}\Big\|_{x=0} = \frac{\partial c_e}{\partial x}\Big\|_{x=L} = 0$	$\dot{\mathbf{c}}_\mathbf{e} = \mathbf{A}^*\cdot\mathbf{c}_\mathbf{e} + \mathbf{B}^*\cdot I$ $\mathrm{y} = \mathbf{C}^*\cdot\mathbf{c}_\mathbf{e} + \mathbf{D}^*\cdot I$
Ohm's law in electrode	$\frac{\partial}{\partial x}\left(\sigma^{eff}\frac{\partial}{\partial x}\varphi_s\right) - j^{Li} = 0$ $-\sigma^{eff}\frac{\partial}{\partial x}\varphi_s\Big\|_{x=0} = -\sigma^{eff}\frac{\partial}{\partial x}\varphi_s\Big\|_{x=L} = \frac{I}{A}$ $\frac{\partial}{\partial x}\varphi_s\Big\|_{x=\delta_-} = \frac{\partial}{\partial x}\varphi_s\Big\|_{x=\delta_- + \delta_{sep}} = 0$	$\frac{\partial}{\partial x}\left(\frac{\partial}{\partial x}\varphi_s\right) = \frac{j^{Li}}{\sigma^{eff}}$ $-\sigma^{eff}\frac{\partial}{\partial x}\varphi_s\Big\|_{x=0} = -\sigma^{eff}\frac{\partial}{\partial x}\varphi_s\Big\|_{x=L} = \frac{I}{A}$ $\frac{\partial}{\partial x}\varphi_s\Big\|_{x=\delta_-} = \frac{\partial}{\partial x}\varphi_s\Big\|_{x=\delta_- + \delta_{sep}} = 0$
Ohm's law in electrolyte	$\frac{\partial}{\partial x}\left(\kappa^{eff}\frac{\partial}{\partial x}\varphi_e\right) + \frac{\partial}{\partial x}\left(\kappa_D^{eff}\frac{\partial}{\partial x}\ln c_e\right) + j^{Li} = 0$ $\frac{\partial}{\partial x}\varphi_e\Big\|_{x=0} = \frac{\partial}{\partial x}\varphi_e\Big\|_{x=L} = 0$	$\frac{\partial}{\partial x}\left(\frac{\partial}{\partial x}\varphi_e\right) + \frac{j^{Li}}{\kappa^{eff}} = 0$ $\frac{\partial}{\partial x}\varphi_e\Big\|_{x=0} = \frac{\partial}{\partial x}\varphi_e\Big\|_{x=L} = 0$
Electrochemical Kinetics	$j^{Li} = a_s i_0\left\{\exp\left[\frac{\alpha_a nF}{RT}\eta\right] - \exp\left[-\frac{\alpha_c nF}{RT}\eta\right]\right\}$	$j^{Li} = a_s i_0\frac{n(\alpha_a + \alpha_c)F}{RT}\eta$
SOC	$SOC = \frac{1}{\delta_-}\int_0^{\delta_-}\frac{(c_{s,ave} - c_{s,\max}Stoi_{100})}{c_{s,\max}(Stoi_{100} - Stoi_0)}dx$	

Appendix B. Cell information and model design parameters

Category	Parameter	Negative electrode	Separator	Positive electrode
Design specifications (geometry and volume fractions)	Thickness, δ (cm)	$94.5*10^{-4}$	$9.5*10^{-4}$	$72.0*10^{-4}$
Lithium-ion concentration	Maximum solid phase concentration, $c_{s,\max}$ (mol cm^{-3})	$52.5*10^{-3}$		$67.2*10^{-3}$
	Stoichiometry at 0% SOC: Stoi0	0.3421		0.8764
	Stoichiometry at 100% SOC: Stoi100	0.8562		0.3268
	Charge-transfer coefficient, α_a, α_c	0.5, 0.5		0.5, 0.5
	Solid phase conductivity, σ (S cm^{-1})	1		0.01
	Electrolyte phase Li + diffusion coefficient, D_e (cm^2 s^{-1})	$1.8*10^{-6}$		$1.8*10^{-6}$
	Solid phase Li + diffusion coefficient, $D_{s,0}$ (cm^2 s^{-1})	$77.1*10^{-6}$		$309.5*10^{-6}$
	Bruggeman's porosity exponent, p	1.5	1.5	1.5
	Electrolyte phase ionic conductivity, κ (S cm^{-1})	$15.8c_e\exp(850c_e^{1.4})$		$15.8c_e\exp(850c_e^{1.4})$
	Li + transference number, t+0	0.363	0.363	0.363
Equilibrium potential	Negative electrode (V)	$U\_(x) = 8.00229 + 5.647x - 12.578x^{1/2} - 8.6322*10^{-4}x^{-1} + 2.1765*10^{-5}x^{3/2} - 0.46016*exp(15*(0.06-x)) - 0.55364*exp(-2.4326*(x-0.92))$, where $x = \bar{c}_{s,surf}/\bar{c}_{s,\max}$		
	Positive electrode (V)	The difference between OCV and the equilibrium potential of the negative electrode		
Side reaction	Equilibrium potential of side reaction, $U_{eq,\ side}$ (V)	0.4		
	Kinetic rate constant for side reaction, k_{side} (A cm mol^{-1})	$0.2*10^{-7}$ [a]		
	Cathodic symmetric factor of side reaction, $\alpha_{c,side}$	0.7		
Lithium plating, stripping	Equilibrium potential of lithium plating, $U_{eq,\ Li}$ (V)	0		
	Exchange current density for lithium plating, $i_{0,Li}$ (A cm mol^{-1})	$0.6*10^{-4}$ [a]		
	Cathodic factor of lithium plating, $\alpha_{c,Li}$	0.7		
	Anodic factor of lithium plating, $\alpha_{c,Li}$	0.3		

References

[1] V. Etacheri, R. Marom, R. Elazari, G. Salitra, D. Aurbach, Challenges in the development of advanced Li-ion batteries: a review, Energy Environ. Sci. 4 (9) (2011) 3243–3262.

[2] S. Zhang, The effect of the charging protocol on the cycle life of a Li-ion battery, J. Power Sources 161 (2) (2006) 1385–1391.

[3] A.J. Salkind, C. Fennie, P. Singh, T. Atwater, D.E. Reisner, Determination of state-of-charge and state-of-health of batteries by fuzzy logic methodology, J. Power Sources 80 (1–2) (1999) 293–300. Jul 1.

[4] C. Mohammad, F. Mohammad, State-of-charge estimation for lithium-ion batteries using neural networks and EKF, IEEE Trans. Ind. Electron. 57 (12) (2010) 4178–4187.

[5] D. Aurbach, M.D. Levi, E. Levi, A. Schechter, Failure and stabilization mechanisms of graphite electrodes, J. Phys. Chem. B 101 (12) (1997) 2195–2206.

[6] P. Verma, P. Maire, P. Novák, A review of the features and analyses of the solid electrolyte interphase in Li-ion batteries, Electrochim. Acta 55 (22) (2010) 6332–6341.

[7] M. Broussely, et al., Main aging mechanisms in Li ion batteries, J. Power Sources 146 (1–2) (2005) 90–96.

[8] A. Victor, J. Fergus, Lithium ion battery anode aging mechanisms, Materials 6 (4) (2013) 1310–1325.
[9] J. Vetter, et al., Ageing mechanisms in lithium-ion batteries, J. Power Sources 147 (1–2) (2005) 269–281.
[10] M. Tang, P. Albertus, J. Newman, Two-dimensional modeling of lithium deposition during cell charging, J. Electrochem. Soc. 156 (5) (2009) 390–399.
[11] H.P. Lin, D. Chua, M. Salomon, H.C. Shiao, M. Hendrickson, E. Plichta, S. Slane, Low-temperature behavior of Li-ion cells, Electrochem. Solid State Lett. 4 (6) (2001) A71–A73.
[12] P. Arora, M. Doyle, R.E. White, Mathematical modeling of the lithium deposition overcharge reaction in lithium-ion batteries using carbon-based negative electrodes, J. Electrochem. Soc. 146 (10) (1999) 3543–3553.
[13] T. Waldmann, B.I. Hogg, M. Wohlfahrt-Mehrens, Li plating as unwanted side reaction in commercial Li-ion cells–A review, J. Power Sources 384 (2018) 107–124.
[14] S.F. Schuster, T. Bach, E. Fleder, J. Müller, M. Brand, G. Sextl, A. Jossen, Nonlinear aging characteristics of lithium-ion cells under different operational conditions, J. Energy Storage 1 (2015) 44–53.
[15] C.R. Birkl, et al., Degradation diagnostics for lithium ion cells, J. Power Sources 341 (2017) 373–386.
[16] K.A. Smith, C.D. Rahn, C.Y. Wang, Control oriented 1D electrochemical model of lithium ion battery, Energy Convers. Manag. 48 (9) (2007) 2565–2578.
[17] Y. Zhao, S.Y. Choe, J. Kee, Modeling of degradation effects and its integration into electrochemical reduced order model for Li (MnNiCo) O2/Graphite polymer battery for real time applications, Electrochim. Acta 270 (2018) 440–452.
[19] R.D. Perkins, A.V. Randall, X. Zhang, G.L. Plett, Controls oriented reduced order modeling of lithium deposition on overcharge, J. Power Sources 209 (2012) 318–325.
[21] X.G. Yang, Y. Leng, G. Zhang, S. Ge, C.Y. Wang, Modeling of lithium plating induced aging of lithium-ion batteries: transition from linear to nonlinear aging, J. Power Sources 360 (2017) 28–40.
[23] J. Li, E. Murphy, J. Winnick, P.A. Kohl, The effects of pulse charging on cycling characteristics of commercial lithium-ion batteries, J. Power Sources 102 (1–2) (2001) 302–309.
[26] M.A. Monem, K. Trad, N. Omar, O. Hegazy, B. Mantels, G. Mulder, Lithium-ion batteries: evaluation study of different charging methodologies based on aging process, Appl. Energy 152 (2015) 143–155.
[28] S.Y. Choe, X. Li, and M. Xiao "Fast charging algorithms based on Li ion concentrations." US Patent No.: 9,197,089, 2015.
[29] Y. Yilin, et al., New fast charging method of lithium-ion batteries based on a reduced order electrochemical model considering side reaction, J. Power Sources 423 (2019) 367–379.
[30] Z. Xinchen, Y.L. Yin, Y. Hu, S.Y. Choe, Electrochemical-thermal modeling of lithium plating/stripping of Li (Ni0. 6Mn0. 2Co0. 2) O2/Carbon lithium-ion batteries at subzero ambient temperatures, J. Power Sources 418 (2019) 61–73.